Modeling and Performance of Electrodynamic Low-Work-Function Tethers with Photoemission Effects

G. Sanchez-Arriaga* and Xin Chen†
Universidad Carlos III de Madrid, Leganés, 28911, Spain

A Low-Work-Function Tether (LWT) is a long conductor, coated with a low work function material, which orbits around a planet with both magnetic field and ionosphere. Depending on the work function W of the coating and the tether temperature T, photoelectron emission can be relevant within the cathodic tether segment. Thus this mechanism needs to be added to the thermionic emission considered in previous works. An emission model for LWTs, including a typical solar photon spectrum, a Fowler-DuBridge law for the photoelectron yield of the coating, and a Richardson-Dushman law for the thermionic emission, is presented, and used to organize the thermionic and photoelectric dominated regimes of LWTs within the $W - T$ plane. This emission model is combined with Orbital-Motion Theory for all the plasma and emitted particles, and the longitudinal bias and current profiles throughout a LWT are determined for typical Low-Earth-Orbit environmental values. Results for the normalized average current, which gauges the efficiency of LWTs, are presented. The study highlights the main electrical, mechanical, and optical properties that should be considered in the design of LWTs, and discusses briefly some promising materials.

*Ramón y Cajal Research Fellow, Bioengineering and Aerospace Engineering Department, Avda. de la Universidad 30, 28911, Leganés, Madrid, Spain
†Visiting Professor (postdoc) Bioengineering and Aerospace Engineering Department, Avda. de la Universidad 30, 28911, Leganés, Madrid, Spain

Nomenclature

A_t = tether cross-sectional area, m^2
$\mathbf{B}$ = ambient magnetic field, T
E_m = motional electric field along the tether, V/m
e = elementary charge, C
$\mathbf{F_L}$ = Lorentz force, N
f_α = distribution function of particle α, s^2/m^5
h_p = Planck constant, m^2kg/s
I = current along the tether, A
J = current density, A/m^2
k_B = Boltzmann constant, m^2kg/s^2K
L^* = length characterizing ohmic effects, m
M_s = spacecraft mass, kg
m_e = electron mass, kg
m_t = tether mass, kg
N_0 = ambient plasma density, $1/m^3$
p_t = tether perimeter, m
R = tether radius, m
r_s = orbital radius of the spacecraft, m
S = Solar energy spectrum, ph/sm^2eV
S_{Sun} = Solar constant, W/m^2
T_e = electron temperature, K
T_i = ion temperature, K
T_{eq} = tether equilibrium temperature, K
T_m = melting temperature, K
$\mathbf{u_t}$ = unit vector along the straight tether
$\mathbf{v}$ = tether-to-plasma relative velocity, m/s
W = work function, eV
x = distance along tether from its anodic end, m
Y = tether photoelectron yield, el/ph
α_{abs} = tether solar absorption
ϵ_{em} = tether emissivity

λ_{De} = electron Debye length, m
μ = standard gravitational parameter, m^3/s^2
Φ_p = tether-to-plasma bias, V
ρ_t = tether density, kg/m^3
σ_B = Stefan-Boltzmann constant, W/m^2K^4
σ_t = tether conductivity, $1/\Omega m$

I. INTRODUCTION

The space debris population near the Earth will increase in the future due to new launches, on-orbit explosions, and accidental collisions. Even without future launches, studies showed that the Low-Earth-Orbit (LEO) debris population will remain relatively constant for the next four decades and will increase noticeably beyond that [1, 2]. Effective means to protect the environment include the deorbit of satellites, payload adapters, and rocket stages at their end-of-life and the active debris removal of the most dangerous objects. Both actions require an active deorbit technology, like chemical and electrical thrusters, or a passive technology, like drag augmentation devices and electrodynamic tethers [3–5].

Bare electrodynamic tethers equipped with plasma contactors, introduced in 1993 [6], can provide a relatively simple and effective solution within a wide range of orbits and spacecraft masses [7][8]. As compared with other technologies, this device has important advantages, which would be enhanced even more if the plasma contactor and its expellant are eliminated. Pursuing this idea, the bare thermionic tether was introduced in 2012 [9]. If the tether is coated with a low-work-function material, then the cathodic contact with the ambient plasma is accomplished by thermionic emission from the tether itself. The operation of the tether is thus fully passive and there is no need for consumable and power supply in deorbit scenarios from LEO. One of the main advantage of using the tether itself for anodic and cathodic contacts is to allow a large collecting/emitting area (even for small tether radius or width) and the reduction of space-charge effects. Preliminary analysis showed that the thermionic tether is a promising device for deorbit payload adapter from Geostationary Transfer Orbits [10].

The charge exchange between the tether and the ambient plasma, and the longitudinal current and voltage profiles along the tether are the main components of the electrical model of the thermionic tether. For an orbital velocity $\mathbf{v}$, the magnetic field $\mathbf{B}$ induces, in the tether reference frame, a motional electric field $\mathbf{v}\times\mathbf{B}$, which drives an electric current along the tether if a closed-circuit electric contact with the environmental plasma is provided. Cathodic and anodic segments develop along such an electrically floating thermionic tether. The tether collects electron along the anodic segment as a giant Langmuir probe and the cathodic segment emits electrons as a giant emissive probe. However, the modeling of the latter is more complex and involves the physical properties of the coating and the ambient plasma.

The first work on thermionic tethers ignored ohmic effects and showed that, in general, the cathodic tether segment has two regions [9]: (i) a segment with space-charge-limited (SCL) emission that extends from the zero bias point B up to an intermediate point B^*, and (ii) a segment between B^* and the tether cathodic end C with full Richardson-Dushman (RD) thermionic emission. The device is said to operate in the *short tether regime* when the full cathodic segment is SCL and in the *long tether regime* if both SCL and RD segments exist. Preliminary models for the precise location of B^* and the plasma/tether charge exchange within BB^* were used in Ref. [9]. Later analysis included ohmic effects [11]. In Ref. [12] a more refined model based on Orbital-Motion Theory (OMT) [13] for the location of B^* was used and the organization of the short and long tether operational regimes were discussed in terms of two key dimensionless parameters.

All the previous works on bare tethers coated with low-work-function materials considered thermionic emission at the cathodic segment. However, our analysis shows that, thanks to the coating, the tether can also act as a photocathode under the natural illumination of the Sun. To the best of our knowledge, this is the first time that a bare electrodynamic tether with photoemission at the cathodic segment is analyzed. Whether photoelectron emission is negligible, comparable, or dominant to thermionic emission, basically depend on tether properties like work function, photoelectric yield, and temperature. For this reason, we will refer to the device as Low-Work-Function Tether, or Low-W Tether (LWT), instead of *thermionic* or *photoelectric* tether. The second novelty of the work is related with the tether/plasma current exchange model, which incorporates full numerical solutions of the Vlasov-Poisson system. This contribution allows to make an assessment of the approximate analytical model used in previous works [9, 11].

The work is organized as following. Section II A introduces a photoemission model for LWT and discusses the operational regimes as a function of the work function and the tether temperature. In Section II B, we modify a recent model for emissive and Langmuir probes [14] to incorporate photoelectric effects. For both anodic and cathodic segments, the current density versus tether bias characteristics, $J(\Phi_p)$, are found by solving self-consistently the Vlasov-Poisson system, considering both thermionic and photoelectric effects. The relations $J(\Phi_p)$ obtained numerically are used to determine the efficiency of LWTs in deorbit scenarios, and to make a critical comparison with previous works [9, 11]. Promising materials for LWT applications are discussed in Sec. IV. The conclusions are summarized in Sec. V.

II. LOW WORK-FUNCTION TETHERS MODEL

For a tether of length L_t, conductivity σ_t, cross-sectional area A_t, and perimeter p_t, the longitudinal

profiles of the current intensity $I(x)$ and the tether-to-plasma bias $\Phi_p(x)$ are governed by [6]

$$\frac{dI}{dx} = p_t \times J\left(\Phi_p\right) \ , \tag{1}$$

$$\frac{d\Phi_p}{dx} = \frac{I}{\sigma_t A_t} - E_m \ , \tag{2}$$

where $J(\Phi_p)$ is the collected/emitted current density (positively defined for electron collection), $x \in [0,\ L_t]$ is the distance along tether from its anodic tip, and $E_m = \mathbf{u_t} \cdot (\mathbf{v} \times \mathbf{B})$ is the motional electric field projection along $\mathbf{u_t}$, which is the tangent unit vector along the straight tether pointing in the direction of the electric current ($\mathbf{I} = \mathbf{I(x)u_t}$). Given the law $J(\Phi_p)$, the integration of Eqs. (1)-(2) with the boundary conditions $I(0) = I(L_t) = 0$ provides the current intensity and bias profiles. From them, one finds the Lorentz force

$$\mathbf{F}_L = \int_0^{L_t} \mathbf{u}_t \times \mathbf{B} I(x) dx \approx \mathbf{u}_t \times \mathbf{B} \int_0^{L_t} I(x) dx, \tag{3}$$

which mainly governs the deorbit performance of the device.

Therefore, the key aspect in the modeling of the tether is the law $J(\Phi_p)$ that is inserted in Eqs. (1)-(2). For the anodic segment, previous works [6, 9] used the orbital-motion-limited (OML) current law. Analytical formulas in the classical [16] and the relativistic [17] (if the probe bias is extremely high like in Jupiter) regimes can be used for tether radius R below a threshold [18]. In the high bias limit ($e\Phi_p/k_BT_e >> 1$, with T_e the plasma electron temperature and k_B the Boltzmann constant), it reads

$$J_{OML} = \frac{eN_0}{\pi}\sqrt{2e\Phi_p/m_e} \ , \tag{4}$$

where m_e is the electron mass, e is the electron charge, and N_0 is the unperturbed plasma density. For the cathodic segment, two issues should be discussed: (i) the emission mechanisms and (ii) the amount of emitted current. Regarding issue (i), previous works considered ion collection and thermionic electron emission [9, 11, 15]. They showed that the thermionic emission dominates against the ion collection, and used the Richardson-Dushman (RD) law

$$J_{th} = -A \times T^2 \exp\left(-\frac{W}{k_B T}\right) \ , \tag{5}$$

with $A = \frac{4\pi m_e e k_B^2}{h_p^3} \approx 1.20 \times 10^6 A m^{-2} K^{-2}$, h_p the Planck constant, and T and W the temperature and work function of tether, respectively. However, emitted electrons result in negative space charge, which suppresses the electric field that accelerates the emitted electrons outwards, or even reverses it at the segment BB*. As advanced by issue (ii), currents emitted by the points at this segment are space-charge-limited (SCL), with a current density $|J_{SCL}| < |J_{th}|$. Previous works [9, 15] used a crude model for J_{SCL} and Ref. [15] presented an asymptotic analysis to predict the position of B^* using OML Theory.

A. Photoelectric emission by LWTs

A coating with low-W materials does not only ease the thermionic electron emission, but can also yield to a relevant photoemission level. The cathodic tether segment, with a negative bias with respect to the ambient plasma, can act as a passive photocathode under the natural illumination of the Sun. However, the modeling of the photocurrent for metal surfaces coated with low-W materials is a difficult and complex task. The photon absorption, the transport of the electrons to the surface and the emission are affected by several factors, including the band structure of the metal, the thickness of the coating, and the angle of incidence and polarization of the light, among others [19, 20]. A reliable determination of the photocurrent, which is highly dependent on the chosen metal/coating combination and the surface treatment, typically requires experiments. In this work, we used a relatively simple but general model and verified that the results are in agreement with previous experiments for specific materials.

The current density of photoelectrons (A/m^2) is given by

$$J_{ph} = -f \times (1 - r_t)\, e \int_0^{\infty} S(E) Y(E) dE \ , \tag{6}$$

where r_t is the LWT reflectivity, $S(E)$ is the energy spectrum of the solar photons (ph/sm^2eV), and $Y(E)$ is the photoelectric yield of the LWT, i.e. the number of emitted electrons per incoming photon (el/ph) for a given photon energy E. The factor f takes into account that only a fraction of the total perimeter is illuminated by the Sun. Panel (a) in Fig. 1 shows the energy spectrum $S(E)$, including the continuous spectrum (solid line) and the discrete lines (triangles), versus the photon energy in electron volts. For energies below and above $4.8eV$ we used the ASTM G173 reference spectra and the data from Ref. [21], respectively.

Regarding the photoelectric yield $Y(E)$ in Eq. 6, we adopted the Fowler-DuBridge law [22, 23]

$$Y(E) = \alpha \times A \times T^2 \times \phi(\frac{E - W}{k_B T}) \ , \tag{7}$$

where ϕ is the Fowler function

$$\phi(x) = \begin{cases} e^x - \frac{e^{2x}}{2^2} + \frac{e^{3x}}{3^2} + \dots & x \le 0 \\ \frac{x^2}{2} + \frac{\pi^2}{6} - \left(e^{-x} - \frac{e^{-2x}}{2^2} + \frac{e^{-3x}}{3^2} - \dots\right) & x \ge 0 \end{cases} \tag{8}$$

with α a constant that depends on the material. For metals, $\alpha \approx 5 \times 10^{-19} - 5 \times 10^{-18} el/ph \times m^2/A$. Hereafter we will (conservatively) assume $\alpha \approx 5 \times 10^{-19} el/ph \times m^2/A$.

Panel (b) in Fig. 1 shows the photoelectric yield per incoming photon versus photon energy using Fowler-DuBridge law and for work function values $W = 1.5, 2.5$ and 3.9 eV. The lines with stars and with circles correspond to experimental data of Copper with a monolayer of Cesium on the surface and Aluminum Oxide,

adapted from Ref. [24] and [25], respectively. For these materials, the authors found work function values equal to 1.55 and 3.9 eV. As shown in the figure, the Fowler-DuBridge law gives a first approximation of $Y(E)$, but accurate and reliable values of $Y(E)$ require experimental tests with the specific metal, coating and surface treatment. For $W = 1.5eV$, our model is very conservative, i.e., it predicts a low value of photoelectrons, because the experimental curve of $Y(E)$ is more than one order of magnitude above the theoretical one. For $3.9eV$, the model is optimistic (conservative) for energies below (above) about $8eV$.

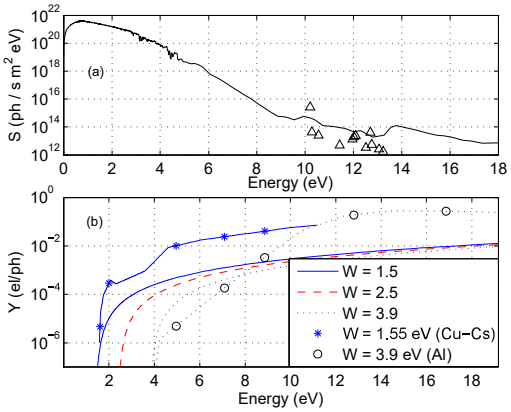

FIG. 1: (a) Solar photon spectrum and (b) photoelectric yield.

Unfortunately, experimental data of the photoelectric yields for the most promising materials with applications to LWTs (see Sec. IV) are not available yet. This issue introduces uncertainties in the results, that we mitigated by presenting parametric studies that vary the LWT temperature and its work function. Figure 2 shows the sum of the photoelectric and the thermionic density currents in logarithm scale versus these two design parameters. The calculation was carried out with Eqs. 5, 6, and 7, $f = r_t = 1/2$ and the solar flux shown in Fig. 1. The $W - T$ relation that gives $J_{th} = J_{ph}$ is shown with a dashed black curve. It separates the parametric domains where the current emission is dominated by photoemission or thermionic emission.

For typical plasma and LWT conditions in LEO, $N_0 = 10^{11}m^{-3}$ and $E_m = 150V/km$, Eq. 4 shows that the maximum collected electron current density for a $1km$-length anodic segment is about $J_{OML} \approx 3.6\times10^{-2}A/m^2$ ($\Phi_p \approx E_mL$). Curiously, according to Fig. 2, a LWT with emission level about this order of magnitude, i.e., $\mid J_{ph} + J_{th} \mid \sim 10^{-2}A/m^2$, has similar contributions from thermionic and photoelectric emissions. Figure 2 also reveals the high sensitivity of the LWT performance with the temperature and the work function. Regarding the former, a balance between radiative cooling and solar absorption gives the LWT equilibrium temperature

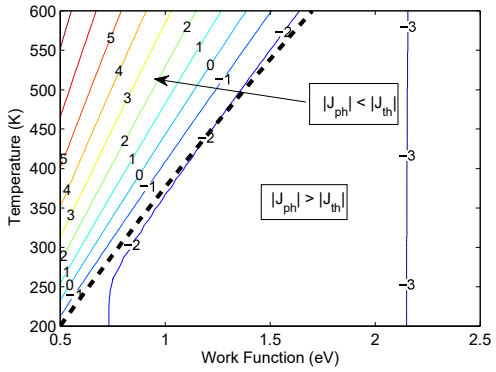

FIG. 2: $log_{10}(\mid J_{ph} + J_{th} \mid)$ versus temperature and work function, with J in A/m^2.

$$T_{eq} = \left(\frac{\alpha_{abs}S_{Sun}}{\pi\epsilon_{em}\sigma_B}\right)^{1/4} \quad (9)$$

with α_{abs} and ϵ_{em} the tether absorptivity and emissivity, $S_{Sun} \approx 1.37kW/m^2$ the solar constant, and $\sigma_B \approx 5.67\times10^{-8}W/m^2K^4$ the Stefan-Boltzmann constant. For $\alpha_{abs} = 0.5$ and $\epsilon_{em} = 0.06$, one finds $T_{eq} \approx 500K$. Joule heating, ignored by this first balance, would increase the equilibrium temperature even more.

B. Plasma/LWT contact

Since the typical length of the LWT is several km and its radius R is about few mm, condition $L_t >> R$ holds. For tapes, the width w_t does also satisfy $w_t << L_t$. This simplifies the LWT/plasma contact model notably because the current density J of a LWT cross section at a particular bias Φ_p can be analyzed as a two-dimensional uniformly-biased Langmuir probe. It is well-known from probe theory that J in Eq. 1 does not generally coincide with J_{OML} and the sum $J_{ph} + J_{th}$ in the anodic and the cathodic segments, respectively. Depending on LWT properties and environmental parameters, a tether cross section could collect electrons *beyond* the OML regime ($J < J_{OML}$) or emit current under SCL conditions ($|J| < |J_{th} + J_{ph}|$).

A rigorous determination of $J(\Phi_p)$ requires OMT, which corresponds to self-consistent solutions of the stationary Vlasov-Poisson system in cylindrical coordinates. In a recent work, this problem was written as an ordinary integro-differential equation and $J(\Phi_p)$ relations were computed numerically for both positive and negative bias [14]. As explained below (see also Appendix A), minor modifications are required to adapt this theory to LWT applications with photoelectric effects.

The first change is related with the boundary conditions of the distribution functions, which should include

the photoelectrons. At the faraway plasma, $r \to \infty$, the electron and ion plasma distribution functions are assumed to be Maxwellian

$$f_{e,i}\left(r \to \infty, v_r, v_\theta\right) = \frac{N_0 m_{e,i}}{2\pi k_B T_{e,i}} \exp\left[-\frac{m_{e,i}\left(v_r^2 + v_\theta^2\right)}{2k_B T_{e,i}}\right] \tag{10}$$

with v_r and v_θ the radial and azimuthal velocities and r the radial distance from the probe axis. At the LWT, $r = R$, the distribution functions of the emitted electrons are assumed to be half-Maxwellian

$$f_{ph,th}\left(R, v_r > 0, v_\theta\right) = \frac{N_{0ph,th} m_e}{\pi k_B T_{ph,th}} \exp\left[-\frac{m_e\left(v_r^2 + v_\theta^2\right)}{2k_B T_{ph,th}}\right] \tag{11}$$

where subscripts ph and th denote electrons emitted through photoelectric and thermionic effects, respectively. For thermionic emission, we will take $T_{th} = T$ in Eq. 11, as commonly done in emissive Langmuir probe studies. Regarding photoemission, an isotropic distribution is realistic for amorphous materials but would not necessarily hold for finely powdered substances [25]. For materials with $W \sim 4 - 5eV$, like Al oxide, the mean kinetic energy is about $k_B T_{ph} \approx 1eV$ [25]. However, experimental results for copper coated with cesium ($W = 1.55eV$) indicates that the mean kinetic energy could be lower [24]. Our calculations will consider $k_B T_{ph} \approx 0.25eV$.

Taking into account Ref. [14] and Eqs. 10-11, one finds that the OMT for a probe with thermionic and photoelectric emissions depends on the following dimensionless parameters

$$\delta_i \equiv \frac{T_i}{T_e}, \quad \delta_{th} \equiv \frac{T_{th}}{T_e}, \quad \delta_{ph} \equiv \frac{T_{ph}}{T_e}, \quad \varphi_p \equiv \frac{e\Phi_p}{k_B T_e}, \tag{12}$$

$$\rho_0 \equiv \frac{R}{\lambda_{De}}, \quad \beta_{th} \equiv \frac{N_{0th}}{N_0}, \quad \beta_{ph} \equiv \frac{N_{0ph}}{N_0} \tag{13}$$

with λ_{De} the electron Debye length. From Eq. 11, one finds the relation

$$J_{ph} = -e\int_0^\infty \int_{-\infty}^{+\infty} v_r f_{ph} dv_r dv_\theta = -N_{0ph} e\sqrt{\frac{2k_B T_{ph}}{\pi m_e}} \tag{14}$$

and a similar equation holds if subscript ph is changed by th. Since J_{th} and J_{ph} are given by Eqs. 5 and 6, the ratios β_{th} and β_{ph} are related with LWT properties - W, T, and $Y(E)$.

Given the set of parameters in Eqs. 12-13, the current density $J(\Phi_p)$ appearing in Eq. 1 is computed as follows. First, the normalized potential profile $\varphi(\rho) = e\Phi/kT_e$ is found by solving Poisson equation

$$\frac{1}{\rho}\frac{d}{d\rho}\left(\rho\frac{d\varphi}{d\rho}\right) = -\rho_0^2\left(n_i - n_e - \beta_{ph} n_{ph} - \beta_{th} n_{th}\right) \tag{15}$$

with $\rho = r/R$. The stationary Vlasov equation with axil-symmetric geometry (round LWT) conserves the energy, the angular momentum and the distribution function, and this can be used to write the normalized particle densities $n_\alpha(\rho)$ as integrals involving $\varphi(\rho)$ (see details in the Appendix A) and Ref. [14]). Equation 15, with the boundary conditions $\varphi(\rho = 1) = \varphi_p$ and $\varphi \to 0$ as $r \to \infty$, is an integro-differential equation that is solved with an iterative numerical algorithm. Once the potential profile $\varphi(\rho)$ is known, the normalized current density $j_{LWT} \equiv J/J_0$ is computed from Eq. A7, with $J_0 = eN_0\sqrt{k_B T_e/2\pi m_e}$ the random electron thermal current.

As an example, we now consider typical environmental values in LEO $k_B T_e = k_B T_i = 0.15eV$, $E_m = 150V/km$, Oxygen ions, and LWT properties $R = 1mm$, $r_t = f = 1/2$, $T = 500K$, $k_B T_{th} = k_B T$, and $k_B T_{ph} = 0.25eV$. These values give the dimensionless parameters $\delta_i = 1$, $\delta_{th} \approx 0.29$, $\delta_{ph} \approx 1.7$, and $\mu_i \approx 29378$. Three relevant cases of plasma densities and coating work function are studied: (i) $N_0 = 10^{11} m^{-3}$ and $W = 1.4eV$ ($\rho_0 \approx 0.11$, $\beta_{th} \approx 2.1$, and $\beta_{ph} \approx 1.4$), (ii) $N_0 = 10^{12} m^{-3}$, and $W = 1.4eV$ ($\rho_0 \approx 0.35$, $\beta_{th} \approx 0.21$ and $\beta_{ph} \approx 0.14$), and (iii) $N_0 = 10^{12} m^{-3}$, and $W = 1.2eV$ ($\rho_0 \approx 0.35$, $\beta_{th} \approx 21.6$, and $\beta_{ph} \approx 0.19$). In cases (i) and (ii) thermionic and photoelectric effects are comparable whereas in case (iii), the one with the higher emission level, thermionic emission is dominant.

For these three cases we computed the $j_{LWT} - \varphi_p$ curve with the Vlasov-Poisson solver (see solid curves in Fig. 3) and with the analytical model presented in [11] but improved with the photoelectric effect (dashed lines). The segment of the $j_{LWT} - \varphi_p$ curve between the two crosses shown in the inset, where we omitted case (iii) for clarity, operates under SCL conditions (non-monotonic potential). As expected, both models match very well, except close to the origin due to space charge effects. Sec. III discusses the importance of such a discrepancy on tether performance and shows that the simplified model of Ref. [9] is adequate for preliminary mission design within a wide range of conditions.

Previous calculations are valid for round tethers at rest and negligible trapped particles populations. Note that the angular momentum of the particles is not conserved for tape tethers or if the relative motion between the plasma and the tether plasma is considered. Trapped particles arise due to collisions or transient phenomena, which would lead to the breakdown of the conservation of f_α or the energy, respectively. Accurate $J(\Phi_p)$ relations for these conditions require the extension of computationally demanding codes like the one presented in Refs. [26–28].

III. ELECTRODYNAMIC PERFORMANCE

After introducing the dimensionless variables $i \equiv I/E_m \sigma_t A_t$, $\phi \equiv \Phi_p/E_m L_t$ and $\xi \equiv x/L_t$, Eqs. 1-2 be-

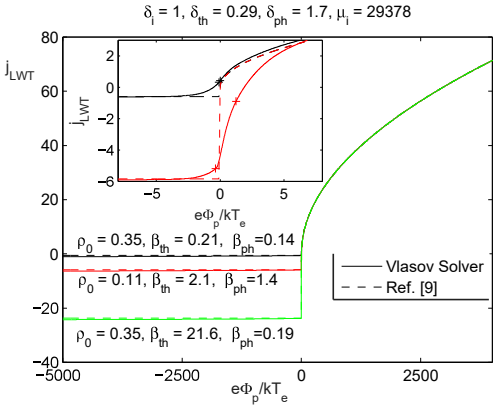

FIG. 3: Normalized current j_{LWT} versus normalized probe bias φ_p for several emission levels

come

$$\frac{di}{d\xi} = \lambda j_{LWT}(\phi), \qquad \frac{d\phi}{d\xi} = i(\xi) - 1 \ , \tag{16}$$

where $\lambda \equiv L_t/L_0$ and $L_0 \equiv E_m \sigma_t A_t / p_t e N_0 \times \sqrt{2\pi m_e / k_B T_e}$. The integration of this set of equations, with the boundary conditions $i(0) = i(1) = 0$ and $j_{LWT}(\varphi_p)$ given by Eq. A7, provides the current and voltage profiles along the tether (note that $\varphi_p = \phi \times e E_m L_t / k T_e$). Once $i(\xi)$ is known, one computes the normalized average current

$$i_{av} = \int_0^1 i(\xi) d\xi = 1 + \phi(1) - \phi(0) \tag{17}$$

that naturally appears in the Lorentz force (see Eq. 3)

$$\boldsymbol{F}_L \approx E_m \sigma_t A_t L_t i_{av} \left(\mathbf{u_t} \times \mathbf{B} \right) \ . \tag{18}$$

The dot product of the spacecraft velocity $\boldsymbol{v} = d\boldsymbol{r}_s/dt$ with its equation of motion $d\boldsymbol{v}/dt = -\mu \boldsymbol{r}_s / r_s^3 + \boldsymbol{F}_L / M_s$ yields [8]

$$\frac{dr_s}{dt} = -2 \frac{r_s^2}{\mu} \frac{m_t}{M_s} \frac{\sigma_t}{\rho_t} E_m^2 i_{av}, \tag{19}$$

where we assumed that the orbit evolves remaining almost circular $v^2 \approx \mu / r_s$ and the straight tether is perfectly aligned with the local vertical. In Eq. 19, r_s is the radius of the orbit, μ the Earth gravitational constant, M_s the spacecraft mass, and $m_t = \rho_t A_t L_t$ and ρ_t the mass and the density of the LWT.

Equation 19 shows that the averaged current intensity i_{av} gauges the efficiency of the tether. Following previous works on bare tethers [6, 29], it will be presented as a function of the ratio L/L^*, where

$$L^* \equiv \left(\frac{2 A_t}{p_t} \right)^{2/3} \times \left(\frac{9 \pi^2 m_e \sigma_t^2 E_m}{128 e^3 N_0^2} \right)^{1/3} \tag{20}$$

is a characteristic dimension that gauges ohmic effects.

Figure 4 shows i_{av} versus L/L^* for $E_m = 150 V/km$, and the parameters discussed in Sec. II B [cases (i)-(iii)]. Similar to Fig. 3, solid lines corresponds to i_{av} values computed with the $j_{LWT} - \varphi_p$ curves obtained from the Vlasov-Poisson solver, and dashed lines with the model of Ref. [9] extended with photoemission. For low emission [case (i)], the differences are notably (above 20%). However, for high emission [case (ii)] the agreement is better than 2% (except in the limit $L/L^* \to 0$, which is not interesting for tether applications). Although the numerical and analytical $j_{LWT} - \varphi_p$ curves exhibit greater differences for high emission because the SCL potential range is broader (see Fig. 3), i_{av} curve show the worst agreement for low emission. This result is explained by the fact that i_{av} is obtained after an integration along the tether. For high emission, OML electron collection for $\varphi_p > 0$ and RD emission at monotonic potential for $\varphi_p < 0$ contribute most to the i_{av} integral and, among such bias ranges, the agreement between both models is good.

It is remarkable that the LWT efficiencies obtained from the numerical $J_{LWT} - \varphi_p$ curves are above the one obtained with the analytical model of Ref. [11]. Therefore, such analytical model is appropriate to carry out conservative analysis in preliminary studies. On the other hand, tether efficiency is enhanced by increasing the emission level (see Fig. 4). The normalized average current i_{av} increases with $\beta_{th} + \beta_{ph}$ and, therefore, with currents J_{th} and J_{ph} (see Eq. 14). LWTs should be manufactured with the lowest achievable work function coating and also with a high photoelectric yield.

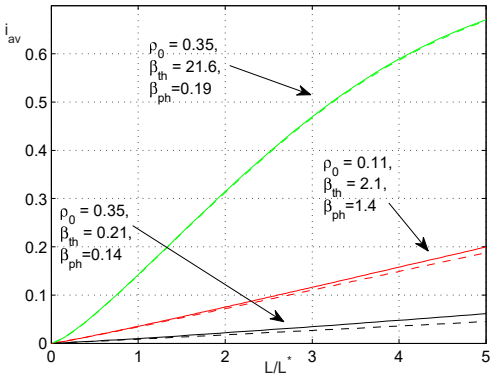

FIG. 4: Normalized averaged current versus L/L^*

Tape tethers exhibit much better performance and are more robust against space debris impacts than round tethers [30]. They are more efficient because, for equal mass and length, tapes have larger perimeters and also smaller L^* due to the factor $(A_t/p_t)^{2/3}$ in Eq. 20. However, in order to find more accurate results, the relation $J(\Phi_p)$ for tapes is needed. This can be done by adapting the 2D stationary Vlasov-Poisson solver of Ref. [31] to include electron emission. An approximate alterna-

TABLE I: Candidates for LWT substrate

Material	ρ_t (kg/m^3)	σ_t $(\Omega^{-1}m^{-1})$	T_m (K)
Al (1100-H19)	2700	3.54×10^7	920
BeCu (C17500)	8600	2.61×10^7	1300

TABLE II: Candidates for LWT coating

Material	$C12A7:e^-$	$BaO-W$	$CeB6$	$LaB6$
W(eV)	0.76, 2.1	2.1	2.5	2.7

tive is to make the perimeter and cross-area replacements $2\pi R \rightarrow 2w_t$ and $\pi R^2 \rightarrow w_t h_t$, with w_t and h_t the width and the thickness of the tape. Note that in the OML regime, the collected current just depends on the perimeter [32], and the same approximation is accurate for tether cathodic points with monotonic potential. However, the limit of validity of OML[18], the emitted current within the SCL regime, and the monotonic/non-monotonic transition φ_p-value must be determined anew for every cross section. As an example, we can make a first estimation of the deorbit performance of a tape of Aluminum with dimensions $L_t = 2km$, $w_t = 2cm$ and $h_t = 50\mu m$, mass $m_t = \rho_t L_t w_t h_t = 5.4kg$, and a spacecraft with mass $M_s = 500kg$ and orbiting at $800km$ of altitude. For the parameters of cases (i)-(iii), one finds $L/L^* \approx 1, 4.8$ and 4.8 and Fig. 4 gives $i_{av} \approx 0.03, 0.06$ and 0.65. Equation 19 gives a decay rate of $2.3, 4.2$ and 46 km/day.

IV. LWT MATERIAL SELECTION

The LWT model presented in Sec. II-III highlights the key design parameters that control the performance of LWTs. This information can be used to select the most promising materials for the tether substrate and its coating. Equation 19 shows that the substrate of the LWT should have a high value of the ratio σ_t/ρ_t. On the other hand, since the electron emission is greatly enhanced by the tether temperature (see Fig. 2), a high melting temperature T_m is also desirable. The properties of two possible materials, Al 1100-H19 and BeCu C17500, are presented in Table I. The decision between these two materials is linked to the properties of the thermionic coating. If the work function is low enough and good emission levels are possible at, say, $T \approx 500K$, then Al is a better choice (due to the larger σ_t/ρ_t ratio). However, if the tether should operate at higher temperature to stimulate the thermionic emission, then a BeCu tether is required due to its higher melting point.

The requirements for the coating are quite demanding because it involves the work function value, optical properties like absorptivity and emissivity and its stability in tough space environment. Table II shows the work function of some thermionic materials. The most promising is the electride $C12A7:e^-$ [33] which combines exceptional characteristics. Although comprised of two insulating oxides (CaO and Al_2O_3, it exhibits high electronic conductivity at room temperature, it is chemically inert and its work function is extremely low. Two different values for its work function, 0.76 eV [34] and 2.1 eV [35], have been measured by different groups. Besides the work function, the final optical properties of the coated tether surface are also critical. In particular, as shown in Eq. 9, the ratio $\alpha_{abs}/\epsilon_{em}$ should be within certain range to guarantee that the LWT operates at the required temperature.

Besides manufacturing issues, there are three testing activities that are required to improve the confidence of the model. First, the curve $J(\Phi_p)$ could be determined experimentally by studying the collected and emitted currents of biased LWT samples in plasma chamber. Second, the photoelectric yield $Y(E)$ may be determined experimentally to predict the response of a LWT irradiated by the sunlight. In third place, testing of the optical properties α_{abs} and ϵ_{em} is also needed. These are the main elements that dictates whether the cathodic contact of the LWT with the plasma is efficient and the feasibility of the concept.

V. CONCLUSION

This work suggests the use of photoelectric effects to achieve a good cathodic contact by bare electrodynamic tethers without using active elements like hollow cathodes. If the tether is coated with a photosensitive compound, then the cathodic segment of the tether would work as a passive photocathode under the natural illumination of the Sun. The extended geometry of Low-Work-function Tethers (LWT), with an enormous disparity between tether length and radius (or width), is appropriate because shielding effects are mitigated while providing quiet large areas. Whether this photoemission is dominant, negligible or comparable with thermionic emission, depends on tether temperature, work function and photoelectric yield. The most important feature of the coating is the work function, which should be low enough to make efficient both emission mechanisms.

Current and voltage profiles along LWTs have been computed with a model that incorporates Orbital-Motion Theory (OMT) throughout the full tether. The calculations, which give a rigorous treatment of the current emission within the space-charge-limited segment, show that previous analytical models are slightly conservative. Therefore, their implementations are fully justified for preliminary mission design purposes. The model introduced in this work could be used by tether flight simulators, aimed at the performance determination of LWTs

with thermionic and photoelectric effects. However, such application needs the development of a large data-base with the current/voltage characteristics obtained from OMT for a wide range of conditions, including tether geometry and environmental variables. Such a work, which would also have applications to emissive and Langmuir probes applied to plasma diagnostics, is in progress.

APPENDIX A: ORBITAL MOTION THEORY RESULTS

For a cylindrical probe immersed at rest in a stationary and collisionless plasma, Vlasov equation conserves the angular momentum, the energy, and the particle distribution functions. These conservation laws are used to write the normalized particle densities, $n_{e,i}(\rho) \equiv N_{e,i}(r)/N_0$ and $n_{ph,th}(\rho) \equiv N_{ph,th}(r)/N_{0ph,th}$, as a function of the normalized radial distance $\rho = r/R$ and electrostatic potential $\varphi(\rho) = e\Phi(r)/kT_e$ (see details in Ref. [14])

$$n_\alpha(\rho) = 2H_\alpha \int_{u^*_{\alpha\rho}}^{\infty} \frac{\exp(-\epsilon_\alpha)}{\pi} \arcsin\left(\frac{l^*_{\alpha\rho}}{l_{\alpha\rho}}\right) d\epsilon_\alpha - H_\alpha \int_{u^*_{\alpha}}^{\infty} \frac{\exp(-\epsilon_\alpha)}{\pi} \arcsin\left(\frac{l^*_{\alpha}}{l_{\alpha\rho}}\right) d\epsilon_\alpha \ . \quad \text{(A1)}$$

In Eq. A1 the subscript α denotes $\alpha = e, i, ph, th$ and we introduced the following functions: $H_{e,i} = 1$, $H_{ph,th} = 2$, $l^2_{\alpha\rho}(\rho, \epsilon_\alpha) = \rho^2 [\epsilon_\alpha - u_{\alpha\rho}(\rho)]$, $u_{i\rho} = \varphi/\delta_i$, $u_{e\rho} = -\varphi$, $u_{ph\rho} = -(\varphi - \varphi_p)/\delta_{ph}$, $u_{th\rho} = -(\varphi - \varphi_p)/\delta_{th}$,

$$u_\alpha \equiv max\{u_\alpha(\rho') : 1 \le \rho' < \infty\} \ , \quad \text{(A2)}$$

$$l_\alpha(\epsilon_\alpha) \equiv min\{l_{\alpha\rho}(\rho', \epsilon_\alpha) : 1 \le \rho' < \infty\} \ , \quad \text{(A3)}$$

and

$$u^*_{\alpha\rho}(\rho) \equiv max\{u_\alpha(\rho')\} \quad \text{(A4)}$$

$$l^*_{\alpha\rho}(\rho, \epsilon_\alpha) \equiv min\{l_{\alpha\rho}(\rho', \epsilon_\alpha)\} \quad \text{(A5)}$$

with $1 \le \rho' \le \rho$ for $\alpha = ph, th$, and $\rho \le \rho' < \infty$ for $\alpha = e, i$. The substitution of Eq. A1 in Poisson equation

$$\frac{1}{\rho}\frac{d}{d\rho}\left(\rho \frac{d\varphi}{d\rho}\right) = -\rho_0^2 (n_i - n_e - \beta_{ph} n_{ph} - \beta_{th} n_{th}) \quad \text{(A6)}$$

yields an integro-differential equation for $\varphi(\rho)$ that should be solved with the boundary conditions $\varphi(1) = \varphi_p$ and $\varphi \to 0$ as $\rho \to \infty$. Once solved, for instance using a finite-element method combined with a Newton algorithm[14], the total current J in Eq. 1 is

$$\frac{J}{J_0} \equiv j_{LWT}(\varphi_p) = \sum_\alpha \frac{2G_\alpha}{\sqrt{\pi}} \int_{u^*_\alpha}^{\infty} l^*_\alpha(\epsilon_\alpha) \exp(-\epsilon_\alpha) \, d\epsilon_\alpha \quad \text{(A7)}$$

with $J_0 \equiv eN_0\sqrt{k_B T_e/2\pi m_e}$ the random electron thermal current. The sum should be extended to the four species ($\alpha = e, i, ph, th$) and we defined the constants $G_i = -\sqrt{\delta_i/\mu_i}$, $G_e = 1$, $G_{th} = -2\beta_{th}\sqrt{\delta_{th}}$, $G_{ph} = -2\beta_{ph}\sqrt{\delta_{ph}}$, and $\mu_i = m_i/m_e$.

ACKNOWLEDGMENTS

GSA work is supported by the Ministerio de Economía y Competitividad of Spain under the Grant RYC-2014-15357

REFERENCES

[1] Liou, J. and Johnson, N., "A Sensitivity Study of the Effectiveness of Active Debris Removal in LEO," *Acta Astronautica*, Vol. 64, Jan. 2009, pp. 236–243. doi:10.1016/j.actaastro.2008.07.009

[2] Liou, J. C., Rossi, A., Krag, H., Xavier James Raj, M., Anilkumar, K., Hanada, T., and Lewis, H., "Stability of the Future of LEO Environment," *Inter-Agency Space Debris Coordination Committee*, Vol. 8, Jan 2013, pp. IADC–12–08, Rev. 1.

[3] Carroll, J. A., "Tether Applications in Space Transportation," *Acta Astronautica*, Vol. 13, No. 4, 1986, pp. 165 – 174. doi: 10.1016/0094-5765(86)90061-5

[4] Grossi, M. D., "Tether History and Historiography," 2^{nd} International Conference on Tether in Space, Consiglio Nazionale delle Ricerche, Venice/Italy, 1987, pp. 3–8.

[5] Cosmo, M. and Lorenzini, E. C., *Tethers in Space Handbook*, NASA CR-97-206807, 3rd ed., 1997.

[6] Sanmartin, J. R., Martinez-Sanchez, M., and Ahedo, E., "Bare Wire Anodes for Electrodynamic Tethers," *Journal of Propulsion Power*, Vol. 9, 1993, pp. 353–360.

[7] Bombardelli, C., Zanutto, D., and Lorenzini, E. C., "Deorbiting Performance of Bare Electrodynamic Tethers in Inclined Orbits," *Journal of Guidance, Control, and Dynamics*, Vol. 36, No. 5, 2013, pp. 1550–1556. doi = 10.2514/1.58428

[8] Sanmartin, J. R., Sanchez-Torras, A., Khan, S. B., Sanchez-Arriaga, G., and Charro, M., "Optimum Sizing of Bare-Tape Tethers for De-Orbiting Satellites at end of Mission," *Advances in Space Research*, Vol. 56, 10 2015, pp. 1485–1492. doi: 10.1016/j.asr.2015.06.030

[9] Williams, J. D., Sanmartín, J. R., and Rand, L. P., "Low Work-Function Coating for an Entirely Propellant-

less Bare Electrodynamic Tether," *IEEE Transactions on Plasma Science*, Vol. 40, May 2012, pp. 1441–1445. doi = 10.1109/TPS.2012.2189589

[10] Sánchez-Arriaga, G., Chen, X., and Lorenzini, E., "Optimal Design and Deorbiting Performance of Thermionic Bare Tethers in Geostationary Transfer Orbits," *Journal of Propulsion and Power*, Ahead of Print. doi: 10.2514/1.B36202

[11] Chen, X. and Sanmartín, J. R., "Bare-tether Cathodic Contact Through Thermionic Emission by Low-Work-Function Materials," *Physics of Plasmas*, Vol. 19, No. 7, July 2012, pp. 073508. doi: 10.1063/1.4736987

[12] Sanmartín, J. R., Chen, X., and Sanchez-Arriaga, G., "Analysis of Thermionic Bare Tether Operation Regimes in Passive Mode," *Physics of Plasmas (Submited)*.

[13] Chen, X., *Low-Work-Function Thermionic Emission and Orbital-Motion-Limited Ion Collection at Bare-Tether Cathodic Contact*, Ph.D. thesis, University Politécnica de Madrid, 2015.

[14] Chen, X. C. and Sanchez-Arriaga, G., "Orbital Motion Theory and Operational Regimes for Cylindrical Emissive Probes ," *Physics of Plasmas, (submited)*.

[15] Chen, X. and Sanmartín, J. R., "Low work-function Thermionic Emission and Orbital-Motion-Limited Ion Collection at Bare-Tether Cathodic Contact," *Physics of Plasmas*, Vol. 22, No. 5, 2015. doi = http://dx.doi.org/10.1063/1.4919945

[16] Laframboise, J. G., *Theory of Spherical and Cylindrical Langmuir Probes in a Collisionless, Maxwellian Plasma at Rest.*, Ph.D. thesis, University of Toronto (Canada)., 1966.

[17] Sánchez-Arriaga, G. and Sanmartín, J. R., "Relativistic Current Collection by a Cylindrical Langmuir Probe," *Physics of Plasmas*, Vol. 19, No. 6, June 2012, pp. 063506. doi: 10.1063/1.4729662

[18] Sanmartín, J. R. and Estes, R. D., "The Orbital-Motion-Limited Regime of Cylindrical Langmuir Probes," *Physics of Plasmas*, Vol. 6, Jan. 1999, pp. 395–405. doi: 10.1063/1.873293

[19] Spicer, W. and Herrera-Gómez, A., "Modern Theory and Applications of Photocathodes ," *Report Nos. SLAC-PUB.6306 and SLAC/SSRL-0042 (unpublished)*, 1993.

[20] Jensen, K. L., Feldman, D. W., Moody, N. A., and O'Shea, P. G., "A Photoemission Model for Low Work Function Coated Metal Surfaces and its Experimental Validation," *Journal of Applied Physics*, Vol. 99, No. 12, June 2006, pp. 124905–124905. doi: 10.1063/1.2203720

[21] Hinteregger, H. E., Hall, L. A., and Schmidtke, G, "Solar XUV Radiation and Neutral Particle Distribution in July 1963 Thermosphere ," *Space Research*, Vol. 5, 1965, pp. 1175.

[22] Fowler, R. H., "The Analysis of Photoelectric Sensitivity Curves for Clean Metals at Various Temperatures," *Phys. Rev.*, Vol. 38, Jul 1931, pp. 45–56. doi: https://doi.org/10.1103/PhysRev.38.45. doi: https://doi.org/10.1103/PhysRev.38.45

[23] Dubridge, L. A., "New Theories of the Photoelectric Effect," *Hermann and Cie, Paris*, 1935.

[24] Berglund, C. N. and Spicer, W. E., "Photoemission Studies of Copper and Silver: Experiment," *Phys. Rev.*, Vol. 136, Nov 1964, pp. A1044–A1064. doi:https://doi.org/10.1103/PhysRev.136.A1044

[25] Grard, R. J. L., "Properties of the Satellite Photoelectron Sheath Derived from Photoemission Laboratory Measurements," *Journal of Geophysical Research*, Vol. 78, June 1973, pp. 2885–2906. doi: 10.1029/JA078i016p02885

[26] Choiniere, E., *Theory and Experimental Evaluation of a Consistent Steady-State Kinetic Model for Two-Dimensional Conductive Structures in Ionospheric Plasmas with Application to Bare Electrodynamic Tethers in Space*, Ph.D. thesis, University of Michigan, 2004.

[27] Sánchez-Arriaga, G., "A Direct Vlasov Code to Study the Non-Stationary Current Collection by a Cylindrical Langmuir Probe," *Physics of Plasmas*, Vol. 20, No. 1, Jan. 2013, pp. 013504. doi: 10.1063/1.4774398

[28] Sánchez-Arriaga, G. and Pastor-Moreno, D., "Direct Vlasov Simulations of Electron-Attracting Cylindrical Langmuir Probes in Flowing Plasmas," *Physics of Plasmas*, Vol. 21, No. 7, July 2014, pp. 073504. doi: 10.1063/1.4889732

[29] Ahedo, E. and Sanmartín, J. R., "Analysis of Bare-Tether Systems for Deorbiting Low-Earth-Orbit Satellites," *Journal of Spacecraft and Rockets*, Vol. 39, March 2002, pp. 198–205. doi: 10.2514/2.3820

[30] Khan, S. B. and Sanmartin, J. R., "Survival Probability of Round and Tape Tethers Against Debris Impact," *Journal of Spacecraft and Rockets*, Vol. 50, May 2013, pp. 603–608. doi: 10.2514/1.A32383

[31] Choiniere, R. and Gilchrist, B. E., "Self-Consistent 2-D Kinetic Simulations of High-Voltage Plasma Sheaths Surrounding Ion-Attracting Conductive Cylinders in Flowing Plasmas," *IEEE Transactions on Plasma Science*, Vol. 35, Feb. 2007, pp. 7–22. doi: 10.1109/TPS.2006.889300

[32] Laframboise, J. G. and Parker, L. W., "Probe Design for Orbit-Limited Current Collection," *Phys. Fluids*, Vol. 16, 1973, pp. 629–636. doi: http://dx.doi.org/10.1063/1.1694398

[33] Toda, Y., Matsuishi, S., Hayashi, K., Ueda, K., Kamiya, T., Hirano, M., and Hosono, H., "Field Emission of Electron Anions Clathrated in Subnanometer-Sized Cages in $[Ca24Al28O64]^{4+}(4e^-)$," *Advanced Materials*, Vol. 16, No. 8, 2004, pp. 685–689. doi: 10.1002/adma.200306484

[34] Rand, L. P., *A Calcium Aluminate Electride Hollow Cathode*, Ph.D. thesis, Colorado State University, 2014.

[35] Toda, Y., Kim, S. W., Hayashi, K., Hirano, M., Kamiya, T., Hosono, H., Haraguchi, T., and Yasuda, H., "Intense Thermal Field Electron Emission from Room-Temperature Stable Electride," *Applied Physics Letters*, Vol. 87, No. 25, Dec. 2005, pp. 254103. doi: 10.1063/1.2149989